

Behaviour of porous ductile solids at low stress triaxiality in different modes of deformation



Viggo Tvergaard

Department of Mechanical Engineering, Solid Mechanics, Technical University of Denmark, DK-2800 Kgs., Lyngby, Denmark

ARTICLE INFO

Article history:

Received 18 November 2014

Received in revised form 12 January 2015

Available online 7 February 2015

Keywords:

Voids
Low stress triaxiality
Large strain plasticity
Contact
Pure shear

ABSTRACT

The effect of low stress triaxiality on ductile failure is investigated for a material subject to pure shear or to stress states in the vicinity of pure shear. Many recent studies of ductile failure under low hydrostatic tension have focused on shear with superposed tension, which can result in simple shear or in stress states near that. A material with a periodic array of voids is subjected to tensile stresses in one direction and compressive stresses in the transverse direction. Numerical solutions for a plane strain unit cell model are obtained numerically. For stress states in the vicinity of pure shear it is found that the voids close up to micro-cracks, and these cracks remain closed during continued deformation, with large compressive stresses acting between crack surfaces. The same type of behaviour is found for different initial sizes of the voids and for cases where the two types of voids in the unit cell have very different initial size. The analyses do not indicate a final failure mode where the stress carrying capacity of the material drops off to zero. In previous analyses for stress states in the vicinity of simple shear such final failure has been predicted, so it appears that the behaviour of a porous ductile material at low stress triaxiality depends a great deal on the mode of deformation.

© 2015 Elsevier Ltd. All rights reserved.

1. Introduction

Under relatively high hydrostatic tension micro-voids contained in a ductile material will tend to grow large during plastic deformation, and ductile failure will occur by coalescence of neighbouring voids (see reviews by [Garrison and Moody, 1987](#); [Tvergaard, 1990](#); [Benzerga and Leblond, 2010](#)). However, recently there has been increasing interest in the behaviour of voids under low stress triaxiality. [Barsoum and Faleskog \(2007a\)](#) have carried out full 3D analyses for shear specimens containing spherical voids in order to model their experiments ([Barsoum and Faleskog, 2007b](#)) on ductile fracture in a double notched tube specimen loaded in combined tension and torsion. In a number of plane strain cell model analyses for a material containing a periodic array of circular cylindrical voids [Tvergaard \(2008, 2009, 2012\)](#) and [Dahl et al. \(2012\)](#) have shown that in stress states similar to simple shear the voids are flattened out to micro-cracks, which rotate and elongate until interaction with neighbouring micro-cracks gives coalescence, and this mechanism has also been found in 3D for initially spherical voids ([Nielsen et al., 2012](#)). Thus, under high stress triaxiality the void volume fraction increases until ductile fracture occurs, whereas the void volume fraction disappears under low

stress triaxiality, as the voids become micro-cracks. In analyses of cases where micro-cracks form it is important to account for the contact between crack surfaces.

An extension of the Gurson model has been proposed by [Nahshon and Hutchinson \(2008\)](#) to be able to describe failure in simple shear where the hydrostatic tension is zero. In this extended model the damage parameter is no longer a geometrically well defined void volume fraction, so this aspect of the model is more like continuum damage mechanics. [Tvergaard and Nielsen \(2010\)](#) have compared predictions of this shear-extended Gurson model with predictions of the micro-mechanical studies ([Tvergaard, 2009](#)) and have found that the trends of the predictions are in good agreement.

A number of recent experimental investigations have considered ductile fracture in shear at a stress triaxiality near zero. Thus, [Bao and Wierzbicki \(2004\)](#), [Beese et al. \(2010\)](#) and [Dunand and Mohr \(2011\)](#), for two different aluminium alloys and a TRIP steel, have used special butterfly specimens to study the effect of the stress triaxiality and of the Lode angle in stress states dominated by shear. [Haltom et al. \(2013\)](#) have used a tubular specimen in tension–torsion while [Chahremaninezhad and Ravi-Chandar \(2013\)](#) have used a modified Arcan test to study the same Al 6061-T3.

In the investigations mentioned above it is characteristic that plastic deformations under low hydrostatic tension are studied

E-mail address: viggo@mek.dtu.dk

under shear loading. When the hydrostatic tension is precisely zero, this mode of deformation is called simple shear. However, deformation under low stress triaxiality can also be applied by subjecting the material to tensile loading in a fixed direction, while compressive loading is applied in the transverse direction. Then material lines along these two loading directions do not at all rotate during the plastic deformations. When the hydrostatic tension is precisely zero, this mode of deformation is called pure shear.

In the present paper a material containing a periodic array of voids is studied under tension in one fixed direction and compression in the transverse direction, so that the modes of deformation considered are either pure shear or in the vicinity of pure shear. The material response is analysed by numerical solutions for a characteristic unit cell model. The main purpose here is to investigate whether or not ductile failure is predicted in these stress states similar to pure shear, analogous to the predictions for stress states similar to simple shear, where the voids are flattened out to micro-cracks, which elongate until interaction with neighbouring micro-cracks gives coalescence.

2. Problem formulation and numerical procedure

The material to be considered here (Fig. 1) has a periodic array of voids, with the initial spacing A_0 in the x^1 -direction and the initial spacing B_0 in the x^2 -direction. Plane strain conditions are assumed. The voids are initially circular cylindrical and staggered, with the radii R_{01} and R_{02} , respectively, so that the voids are located in opposite corners of the rectangular unit cell in Fig. 1. Finite strains are accounted for and the analyses are based on a convected coordinate Lagrangian formulation of the field equations, with a Cartesian x^i coordinate system used as reference and with the displacement components on reference base vectors denoted by u^i . The metric tensors in the reference configuration and the current configuration, respectively, are g_{ij} and G_{ij} with determinants g and G , and $\eta_{ij} = 1/2(G_{ij} - g_{ij})$ is the Lagrangian strain tensor. In terms of the displacement components u^i on the reference base vectors the Lagrangian strain tensor is

$$\eta_{ij} = \frac{1}{2} (u_{i,j} + u_{j,i} + u_{,i}^k u_{k,j}) \quad (1)$$

where $(\cdot)_{,j}$ denotes covariant differentiation in the reference frame. The contravariant components τ^{ij} of the Kirchhoff stress tensor on the current base vectors are related to the components of the Cauchy stress tensor σ^{ij} by $\tau^{ij} = \sqrt{G/g} \sigma^{ij}$. A finite strain formulation for a J_2 flow theory material with the Mises yield surface is applied, where the incremental stress–strain relationship takes the form $\dot{\tau}^{ij} = L^{ijkl} \dot{\eta}_{kl}$, with the instantaneous moduli specified in

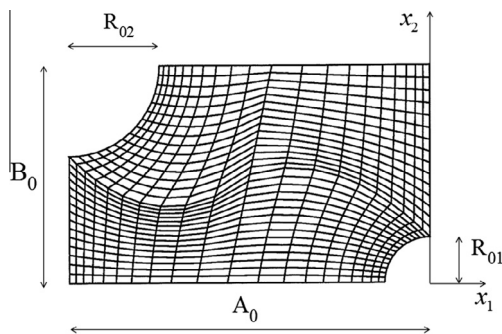


Fig. 1. A unit cell used to analyse a material with a periodic array of circular cylindrical voids. Example of an initial mesh is shown for a case with $B_0/A_0 = 0.6$, $R_{01}/A_0 = 0.125$ and $R_{02}/A_0 = 0.25$.

(Hutchinson, 1973; Tvergaard, 1976). The true stress–logarithmic strain curve in uniaxial tension is taken to follow the power law

$$\varepsilon = \begin{cases} \sigma/E, & \sigma \leq \sigma_Y \\ (\sigma_Y/E)(\sigma/\sigma_Y)^{1/N}, & \sigma \geq \sigma_Y \end{cases} \quad (2)$$

with Young's modulus E , the initial yield stress σ_Y and the power hardening exponent N . Poisson's ratio is ν .

The material is subjected to tensile loading in the x^2 -direction, such that average true stress Σ_{22} in the vertical direction is a principal stress. Thus, also the average true stress Σ_{11} in the x^1 -direction is a principal stress. The numerical calculations are carried out such that a fixed stress ratio is prescribed

$$\Sigma_{11}/\Sigma_{22} = \kappa \quad (3)$$

and in most cases the value of the constant κ is prescribed as negative (where the value -1 corresponds to pure shear). With the assumed symmetries of the material geometry and with the loading applied in the vertical and horizontal directions the material lines along the coordinate axes will remain straight throughout the deformation. Thus, the boundary conditions to be satisfied along all four edges of the rectangular unit cell are standard symmetry conditions. The average logarithmic strains in the two coordinate directions are denoted ε_1 and ε_2 , respectively.

When the hydrostatic tension is sufficiently low in the present computations, the voids are going to close up to form micro-cracks, so that contact conditions are needed for the points on the void surface. For each nodal point on the void surface the displacements are checked relative to the location of the edge lines crossing the void. If the displacements exceed such a symmetry line, this surface point overlaps with the symmetrically located surface point in the neighbouring unit cell, and this marks the onset of surface contact at that particular nodal point. From then on the displacement normal to the edge of the unit cell is prescribed to be equal to that of the edge line. Subsequently, when contact has been established in a nodal point on the void surface, the value of the compressive nodal force on the symmetry plane is checked, and if this force becomes tensile, the contact is released, so that the void can start opening up again. Friction during contact is not an issue here, as the symmetry line through each void means, that there is no sliding between the void surfaces.

It is noted that initially computations have been carried for only half the unit cell, i.e. a cell with the length $A_0/2$ in the x^1 -direction and the height B_0 in the x^2 -direction, containing only part of one void. However, the staggered void arrangement in Fig. 1 has been preferred, since this promotes interaction between the voids by a region of intense shear strains, and this also allows for considering different size voids.

The numerical solutions for the fields inside the unit cell are obtained by a linear incremental solution procedure, based on the incremental principle of virtual work. On the void surfaces zero nominal tractions are specified, until contact occurs as described above. The displacement fields are approximated in terms of 8-noded isoparametric elements, and volume integrals in the principle of virtual work are carried out by using 2×2 point Gauss integration within each element. An example of a mesh used for some of the numerical analyses is shown in Fig. 1.

In each increment an increasing average strain ε_2 is prescribed in the vertical direction, and the increment of the transverse strain is calculated such that the prescribed stress ratio (3) remains satisfied. This is carried out by using a Rayleigh Ritz-finite element method (Tvergaard, 1976).

Remeshing is used a few times in each computation to avoid severe mesh distortion. The remeshing procedure applied was first introduced in one of the authors finite strain programmes by Pedersen (1998), and has been further developed in (Tvergaard,

1997). The values of field quantities in the integration points of the new mesh are determined by interpolation in the old mesh. To do this, it is necessary to determine the location of each new nodal point and integration point in the old mesh, i.e. the element number and the appropriate values of the local coordinates ξ and η inside that element, where the region of the element is specified by $-1 \leq \xi \leq 1$ and $-1 \leq \eta \leq 1$. This is done by repeated use of a Newton–Raphson iteration.

3. Results

In the computations to be presented here the material parameters are taken to be $\sigma_Y/E = 0.002$, $\nu = 0.3$ and $N = 0.1$. Different values are considered for the initial aspect ratio of the region analyzed, B_0/A_0 , the initial void radii, and the stress ratio κ in (3).

In the first results shown the initial radii of the two cylindrical voids are taken to be nearly identical, with $R_{02}/R_{01} = 1.01$, while the unit cell aspect ratio is $B_0/A_0 = 0.6$, and $R_{01}/A_0 = 0.25$. Fig. 2 shows calculated stress strain curves for four different values of the stress ratio $\kappa = \Sigma_{11}/\Sigma_{22}$ and due to the symmetries of the loading and of the periodic pattern of holes represented by the unit cell, the macroscopic shear stress is $\Sigma_{12} = 0$.

Fig. 3 shows the current deformed meshes for the computation with $\Sigma_{11}/\Sigma_{22} = -0.5$ in Fig. 2 at two different stages of the deformation, specified by the logarithmic strain values $\varepsilon_2 = 0.29$ and $\varepsilon_2 = 0.61$. For the same two deformed unit cells Fig. 4 shows the contours of effective plastic strain. Starting from circular cylindrical shapes, the voids elongate significantly in the tensile direction, and their shapes remain essentially identical. With tensile loading in the x^2 -direction it is clear that stress and strain concentrations will develop early on at the void surfaces where the ligament length is smallest, i.e. where the void surfaces cut the horizontal edges of the unit cell (see Fig. 1). These two regions of elevated strains are still visible in Fig. 4a, even though the voids are strongly elongated at this stage. Strong interaction between the two voids is seen by the band of relatively high strains connecting the voids in Fig. 4a. When the voids start to close up to form micro-cracks, at $\varepsilon_2 = 0.36$, the slope of the stress strain curve in Fig. 2 increases significantly and then develops on a higher stress level than indicated by the first part of the curve. The increase of slope starts when the first points of the void surface get in contact, and subsequently the contact regions increase until full contact is obtained as illustrated in Figs. 3 and 4b. At this stage rather large compressive stresses act normal to the micro-cracks, at all points of the crack surfaces, so there is no indication that the cracks would start to interact in a way leading to a stress maximum.

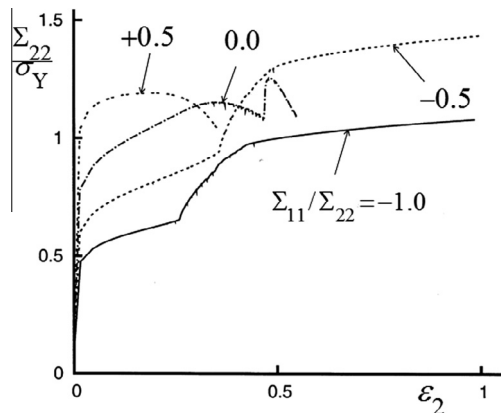


Fig. 2. Curves of average true tensile stress Σ_{22} vs. logarithmic strain ε_2 for $B_0/A_0 = 0.6$, $R_{01}/A_0 = 0.25$, $R_{02}/R_{01} = 1.01$ and various values of $\Sigma_{11}/\Sigma_{22} = \kappa$.

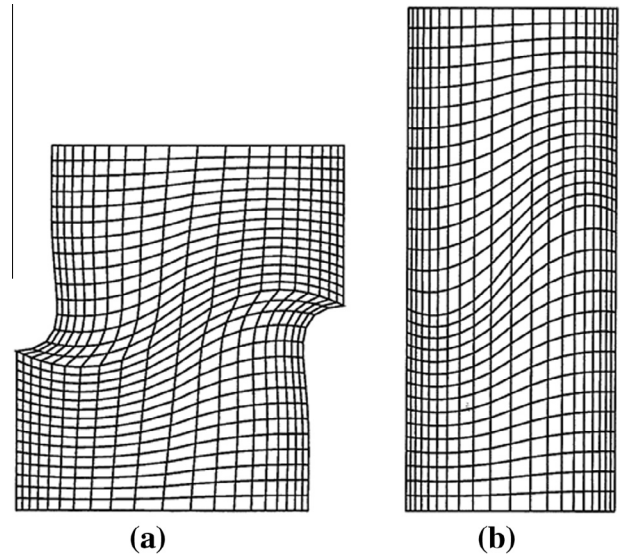


Fig. 3. Deformed unit cells showing the current deformed meshes for the computation with $\Sigma_{11}/\Sigma_{22} = \kappa = -0.5$ in Fig. 2. (a) At $\varepsilon_2 = 0.29$. (b) At $\varepsilon_2 = 0.61$.

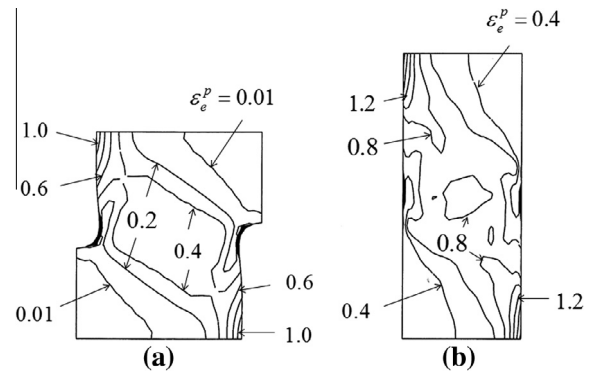


Fig. 4. Deformed unit cells with contours of effective plastic strain corresponding to the computation with $\Sigma_{11}/\Sigma_{22} = \kappa = -0.5$ in Fig. 2. (a) At $\varepsilon_2 = 0.29$. (b) At $\varepsilon_2 = 0.61$.

When the voids are closed, as in Figs. 3b and 4b, the locations of the crack tips are still seen in the deformed mesh, since 15 elements are used along each crack, and also 15 elements are used along the unbroken ligaments, even after a few remeshings. After that these cracks are completely closed the normal contact stresses on the crack surfaces gradually approach a uniform level equal to Σ_{11} .

Fig. 5 shows contours of effective plastic strain like those in Fig. 4, but now for the computation with $\Sigma_{11}/\Sigma_{22} = 0.0$. As illustrated by the corresponding curve in Fig. 2 this case first shows a

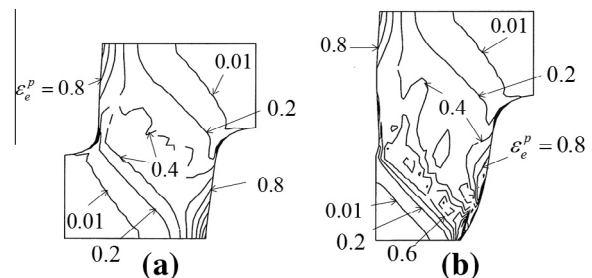


Fig. 5. Deformed unit cells with contours of effective plastic strain corresponding to the computation with $\Sigma_{11}/\Sigma_{22} = \kappa = 0.0$ in Fig. 2. (a) At $\varepsilon_2 = 0.30$. (b) At $\varepsilon_2 = 0.46$.

maximum stress, as necking starts to develop in the unit cell. The preferred necking mode is asymmetric, so that one of the voids closes to a micro-crack, while the other void grows rapidly. At first contact on the micro-crack surface the load starts to increase with a steep slope, then reaches a secondary maximum before the load again starts to decay during the necking mode seen in Fig. 5b. The stage shown in Fig. 5a is at $\varepsilon_2 = 0.30$, slightly before the first maximum on the curve, so here the growth of the two voids is still nearly equal. In Fig. 5b the average strain is $\varepsilon_2 = 0.46$, which is just before the first contact during micro-crack closure, so just before the steep increase in the slope of the stress–strain curve. The void closing up to a micro-crack in Fig. 5b is that with initial radius R_{02} , while the void with initial radius R_{01} keeps growing by necking of the ligament between this void and the neighbour void of the same type in the neighbour cell model.

The curve for $\Sigma_{11}/\Sigma_{22} = -1.0$ in Fig. 2 represents a case near pure shear, with approximately zero stress triaxiality. Here the behaviour is very close to that illustrated in Figs. 3 and 4, with the difference that crack closure occurs at a smaller strain than that found for $\Sigma_{11}/\Sigma_{22} = -0.5$, due to the larger compressive stress in the x_1 direction. Neither of these cases show any tendency towards failure by interaction of the cracks. On the other hand, the curve for $\Sigma_{11}/\Sigma_{22} = 0.5$ in Fig. 2 corresponds to a rather high stress triaxiality, where both voids grow. Beyond the stress maximum one of the voids essentially stops growing, while the other void grows larger, but there is no tendency towards micro-crack formation at any of the two voids.

For comparison Fig. 6 shows a deformed unit cell subject to shear, taken from Tvergaard (2015). This result for shearing under a low positive stress triaxiality is chosen because the strain contours are included, but it is known from Tvergaard (2009, 2012) that very similar behaviour is found in simple shear, where the hydrostatic tension is zero. The elongated voids in Fig. 6 simulate closed cracks with frictionless sliding, using a pseudo contact condition, which has been explained in the previous papers. But the point of main interest is that in the case of Fig. 6 the applied macroscopic shear stress passes through a maximum, and Fig. 6b is well beyond this maximum, whereas the curves for the low stress triaxialities in Fig. 2 do not show a maximum macroscopic stress. The failure mechanism in cases like Fig. 6 is that the neighbouring cracks rotate and elongate in the shear field, so that they develop increasing overlap with the neighbouring micro-cracks. Then large strains develop only on one side of the crack tip, towards the neighbouring overlapping crack, and finally failure occurs by necking of the ligament between them. By contrast, in cases like Figs. 3b and 4b no further overlap of neighbouring micro-cracks develops once the voids have closed up to micro-cracks, since then the micro-cracks just elongate at the same speed as the elongations in all the surrounding material.

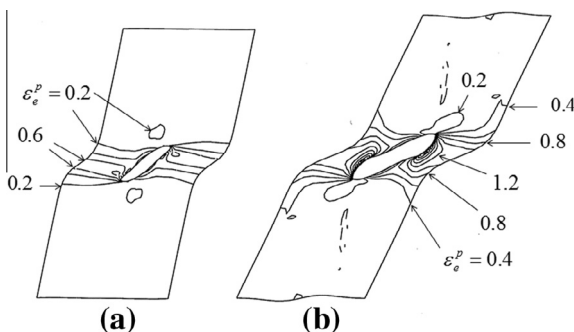


Fig. 6. Deformed unit cells with contours of effective plastic strain corresponding to a computation with a circular cylindrical void. The load is simple shear with a small superposed hydrostatic tension. (a) At $F_{12} = 0.31$. (b) At $F_{12} = 0.69$. (From Tvergaard, 2014b).

Both the present analyses and those in Tvergaard (2009, 2012) consider plane strain conditions. Both in the present analyses for pure shear where $\Sigma_{11} = -\Sigma_{22}$ and $\Sigma_{12} = 0$, and in analyses for simple shear where Σ_{12} is prescribed while $\Sigma_{11} = \Sigma_{22} = 0$ the value of the Lode parameter is zero. But the cracks in the two cases do not behave the same way, since in simple shear the crack surfaces slide against each others, and material flows around the crack tips. In the present pure shear calculations there is no sliding between crack surfaces and no material flow around crack tips.

Fig. 7 shows curves like those in Fig. 2, computed for the same initial geometry of the unit cell, and the curve for $\Sigma_{11}/\Sigma_{22} = 0.0$ is identical to that in Fig. 2. The other two curves are included to focus on how quickly the mode of behaviour changes with the change of stress state. It is seen that for $\Sigma_{11}/\Sigma_{22} = 0.25$ the change has already occurred to the full necking behaviour without micro-crack formation that was also found for $\Sigma_{11}/\Sigma_{22} = 0.5$ in Fig. 2. For $\Sigma_{11}/\Sigma_{22} = -0.25$ the increase in the slope of the curve is not as sudden as was found for two of the curves in Fig. 2. Here, the void with initial radius $0.2525A_0$ experiences surface contact at $\varepsilon_2 = 0.44$, and the slope increases somewhat. Then, at $\varepsilon_2 = 0.47$ contact starts at the other void, leading to the steep increase in slope shown in Fig. 7. Subsequently, contact quickly spreads to most of the two void surfaces, but at the end of the computation there are still small regions left without contact in both voids.

It should be emphasised here that a failure mode is found for the computations leading to a stress maximum in Figs. 2 and 7. In these cases failure is predicted in the form of necking between neighbouring voids, as is seen developing in Fig. 5b. On the other hand, no such stress maximum is predicted in the cases of sufficiently large compressive transverse stress. In the case of Fig. 5 the void volume fraction is increasing, while in Fig. 4 the void volume fraction becomes zero.

A comparison with predictions by the model of Nahshon and Hutchinson (2008) for simple shear type loading has been carried out by Tvergaard and Nielsen (2010). As in simple shear with zero mean stress, also in pure shear the damage parameter in this model will keep growing, but only due to the extra added damage term, like in continuum damage mechanics.

The initial angle between the two voids in the unit cell (Fig. 1) has so far been arbitrarily chosen by using the initial aspect ratio $B_0/A_0 = 0.6$. The effect of this parameter is studied in Fig. 8 by comparing results for a number of different values of B_0/A_0 . As in the previous figures, the initial ratio of the void radii is $R_{02}/R_{01} = 1.01$, with $R_{01}/A_0 = 0.25$. The curves are computed for $\Sigma_{11}/\Sigma_{22} = -1.0$,

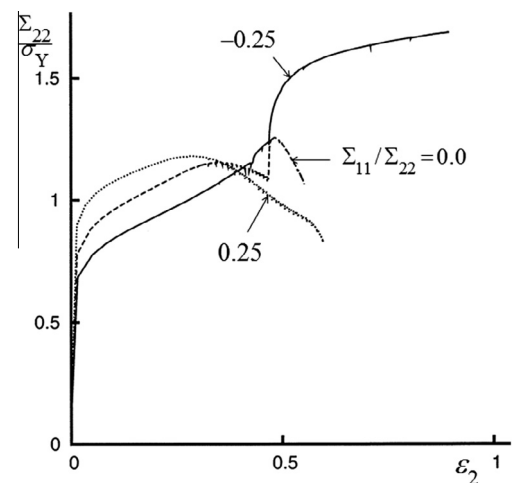


Fig. 7. Curves of average true tensile stress Σ_{22} vs. logarithmic strain ε_2 for $B_0/A_0 = 0.6$, $R_{01}/A_0 = 0.25$, $R_{02}/R_{01} = 1.01$ and various values of $\Sigma_{11}/\Sigma_{22} = \kappa$.

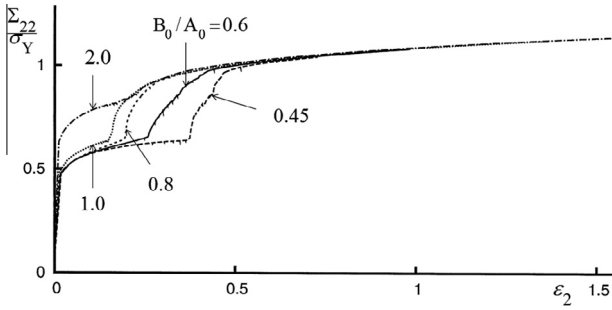


Fig. 8. Curves of average true tensile stress Σ_{22} vs. logarithmic strain ϵ_2 for $\Sigma_{11}/\Sigma_{22} = \kappa = -1.0$, $R_{01}/A_0 = 0.25$, $R_{02}/R_{01} = 1.01$ and various values of B_0/A_0 .

with approximately zero stress triaxiality, and thus the curve for $B_0/A_0 = 0.6$ in Fig. 8 is identical to that for $\Sigma_{11}/\Sigma_{22} = -1.0$ in Fig. 2. It is seen that in all five cases illustrated in Fig. 8 the shapes of the curves are like the predictions for the stress ratios -1.0 and -0.5 in Fig. 2. Thus, in all cases the unit cells deform in a manner corresponding to that shown in Figs. 3 and 4, where the voids flatten out until there is void surface contact so that two micro-cracks have formed. As was found before, rather large compressive stresses act normal to the micro-cracks at all points of the crack surfaces. The main difference between the five curves in Fig. 8 is the location of the point where the slope starts to increase rapidly, i.e. the point where void surface contact initiates, leading to the micro-cracks. After some further deformation, at a strain around $\epsilon_2 = 0.5$, the curves nearly coincide, as the behaviour approaches that for a uniformly stressed specimen with $\Sigma_{11}/\Sigma_{22} = -1.0$.

Computations have also been carried out for smaller initial voids, i.e. for $R_{01}/A_0 = 0.125$ with $R_{02}/R_{01} = 1.01$, see Fig. 9. As in Fig. 2 the aspect ratio of the unit cell is chosen to be $B_0/A_0 = 0.6$, and the values of the stress ratios considered are the same as those in Fig. 2. It is seen that in the initial stages, at rather small strains, all four curves reach higher stress levels than those found in Fig. 2, because the stress levels are reduced by the presence of voids, and this reduction is larger the voids. On the other hand, for $\Sigma_{11}/\Sigma_{22} = -1.0$ and $\Sigma_{11}/\Sigma_{22} = -0.5$ there is a relatively smaller increase of the stress level when the voids become micro-cracks. In the case of $\Sigma_{11}/\Sigma_{22} = 0.5$ it takes more straining before the load drops rapidly, as this occurs due to necking of the ligament between voids, which develops less rapidly when the initial voids are smaller.

The unit cell (Fig. 1) also allows for big differences between the initial sizes of the two types of voids. To investigate the effect of such configurations computations have been carried out for $R_{02}/R_{01} = 2.0$ with $R_{01}/A_0 = 0.125$, while still using the aspect ratio $B_0/A_0 = 0.6$ as in most of the previous figures. Thus, the initial mesh used here is exactly that illustrated in Fig. 1. Fig. 10 shows curves computed for five different values of the stress ratio, where four of the values are those also considered in Figs. 2 and 9. The additional value, $\Sigma_{11}/\Sigma_{22} = -1.5$, is studied just to confirm that increased transverse compression does not change the general picture. The three curves for the stress ratios -0.5 , -1.0 and -1.5 show the type of behaviour also found in Figs. 2 and 7–9 for negative stress ratios. The last two curves show effects of the development of necking, similar to those described in relation to Figs. 2 and 9. The curve for $\Sigma_{11}/\Sigma_{22} = -0.5$ shows the expected steep increase in slope at the occurrence of first void surface contact, i.e. at $\epsilon_2 = 0.30$, but afterwards the curve shows some waviness, which will be further discussed in relation to the next figure.

Two different deformed stages of the unit cell for $\Sigma_{11}/\Sigma_{22} = -0.5$ in Fig. 10 are illustrated in Fig. 11, with contours of effective plastic strain included, as in Fig. 4. The two stages are at the

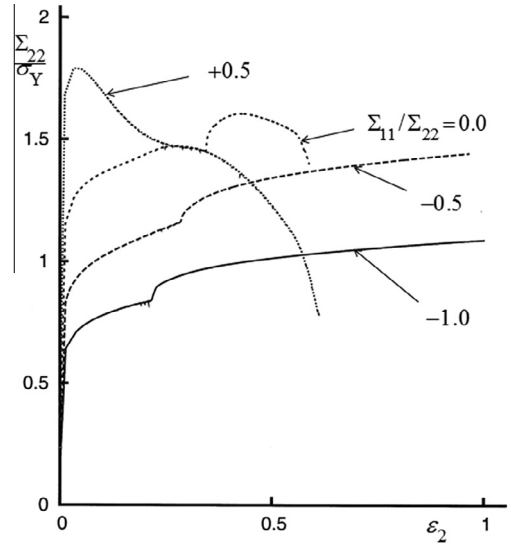


Fig. 9. Curves of average true tensile stress Σ_{22} vs. logarithmic strain ϵ_2 for $B_0/A_0 = 0.6$, $R_{01}/A_0 = 0.125$, $R_{02}/R_{01} = 1.01$ and various values of $\Sigma_{11}/\Sigma_{22} = \kappa$.

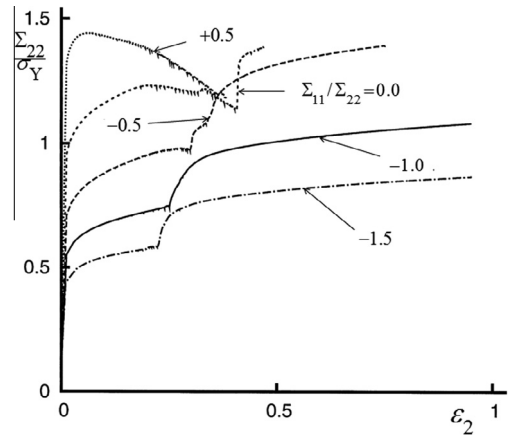


Fig. 10. Curves of average true tensile stress Σ_{22} vs. logarithmic strain ϵ_2 for $B_0/A_0 = 0.6$, $R_{01}/A_0 = 0.125$, $R_{02}/R_{01} = 2.0$ and various values of $\Sigma_{11}/\Sigma_{22} = \kappa$.

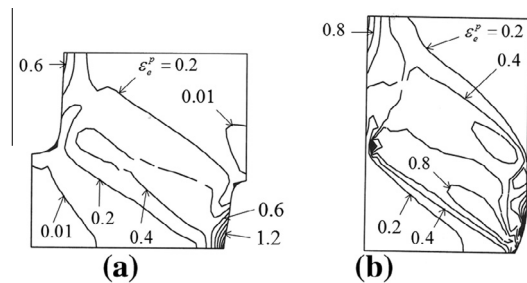


Fig. 11. Deformed unit cells with contours of effective plastic strain corresponding to the computation with $\Sigma_{11}/\Sigma_{22} = \kappa = -0.5$ in Fig. 10. (a) At $\epsilon_2 = 0.20$. (b) At $\epsilon_2 = 0.39$.

average strains $\epsilon_2 = 0.20$ and $\epsilon_2 = 0.39$. In Fig. 11a, well before any void surface contact, both voids are much elongated, and it is seen that the smaller void with initial radius $0.125A_0$ has resulted in more intense straining near the void surface than the other void. Void surface contact starts on the larger void, at $\epsilon_2 = 0.30$, which develops rather quickly into a fully closed micro-crack. Fig. 11b is very close to this stage, where the larger void has become a

micro-crack, and it is seen that void closure has also developed over a good part of the smaller void. However, near the symmetry surface at $x^2 = 0$ contact has not yet occurred, and this contact region grows only slowly. In fact, at the end of the curve shown in Fig. 10, near $\varepsilon_2 = 0.74$, a very small part of the void is still not closed.

The present computations do not indicate a failure mode at low stress triaxiality such as $\Sigma_{11}/\Sigma_{22} = -1.0$, which is close to pure shear. This is different from the situations close to simple shear, considered by Tvergaard (2008, 2009, 2012) and Dahl et al. (2012), where the average shear stress starts to decay rapidly, when coalescence of neighbouring micro-cracks develops by necking of the ligaments between them. Furthermore, a recent study (Tvergaard, 2014) has shown that these materials will tend to fail even earlier, as bifurcation into a shear band occurs near the location of the maximum average shear stress.

For stress states like $\Sigma_{11}/\Sigma_{22} = -1.0$ the deformation modes analysed in the present paper do not indicate failure. After that the voids have closed up to micro-cracks high compressive stresses are present across the crack surfaces in contact, and the stress state approaches more and more that of a uniformly stressed material. If an instability would occur, such as a shear band formation, that could represent a failure mode.

To obtain an indication of a possible shear band instability, influenced by the presence of the cracks, a simplified problem can be considered for pure shear, where no stress maximum has been predicted. Here, the problem is simplified by assuming that the micro-cracks are present from the beginning, and that they have equal length. Then the stress state is uniform throughout the solid with the constant ratio -1.0 between the principal true stresses. For this situation an approximate shear band analysis like that in (Tvergaard, 2014) can be carried out by searching for a periodic pattern of deformations with some shear, which could represent the deformations inside a shear band. Such analyses have been attempted, assuming frictionless sliding between the micro-crack surfaces, but no bifurcation has been found.

It should be emphasised that larger unit cells with many voids within the cell may give differences from the predictions found here. The location of the two types of voids here on symmetry lines makes it easy to do precise contact analyses during close up to micro-cracks. For a more complex problem with internal voids there is no guarantee that the micro-cracks would become exactly parallel to a macroscopic principal stress, and a contact analysis would make use of approximations such as the pseudo contact condition in Tvergaard (2009, 2012) or a cohesive zone model.

Only one hardening level is considered here, $N = 0.1$, to map out what is predicted for one type of material. But generally, based on other localization results, it is expected that more high hardening materials will give later localization, while non-hardening will lead to slip bands.

Shear bands in a homogeneously deformed material under plane strain have been studied by Hill and Hutchinson (1975). For a hardening elastic–plastic solid with a smooth yield surface, as the J_2 flow theory material considered here, these results show that loss of ellipticity of the governing equations will not occur, even at huge strains, and therefore bifurcation in a shear band will not occur. However, if a different set of elastic–plastic constitutive equations was assumed, such as J_2 corner theory (Christoffersen and Hutchinson, 1979), loss of ellipticity would occur earlier. At the vertex a finite strain J_2 deformation theory is often taken to represent the moduli, either in a hypoelastic version (Stören and Rice, 1975) or a truly elastic version (Hill, 1970). For a power hardening J_2 corner theory material the critical strain for shear bands is (Tvergaard and Hutchinson, 1981)

$$\varepsilon_c = (N(q - N))^{1/2} \quad (4)$$

where $q = 1$ for the hypoelastic theory and $q \approx 1.13$ for the truly elastic theory, leading to the critical strains 0.3 and 0.322, respectively, for $N = 0.1$. Therefore, if J_2 corner theory had been applied here, instead of J_2 flow theory, the deformed unit cells would have been strongly affected by localised shear bands long before the end of the present computations.

Interesting results related to the present study have been found in a recent paper by Song et al. (2015). They use homogenisation theory for a porous metal to account for the evolution of both void shape and void orientation, and based on this model they apply conditions for loss of strong ellipticity to predict strain localization. Their model does not account for the contact when voids close up to micro-cracks at low stress triaxiality. However, for a high void volume fraction (10%) they find localization in simple shear before the voids have closed up, but in pure shear they find no localization. Their approach is very different from the one used in the present paper, but it is interesting that the results are the same.

4. Discussion

In recent years, several different authors have investigated ductile fracture of metals at low stress triaxiality, either experimentally or by computational models. This range of stress states is of particular interest because voids will collapse to micro-cracks rather than grow, so that the often observed ductile fracture mode, with growing void volume fraction until coalescence, will not occur. Practically all these investigations have considered shear with superposed tension, which corresponds to stress states near simple shear. The present investigation considers low triaxiality stress states near pure shear. While computations for collapsed voids in simple shear have shown a clear failure mode by coalescence of micro-cracks, the present studies do not indicate a ductile failure mode for a void containing ductile material subject to pure shear.

The representative unit cells considered here contain initially part of two voids. As expected both voids develop into micro-cracks when the hydrostatic tension is near zero, and these cracks remain closed during the subsequent deformation with a high compressive stress acting between crack surfaces. When the plane strain tensile test is carried out with less transverse compression, or even transverse tension, so that there is a positive stress triaxiality, a transition is predicted to a mode where failure occurs by necking of ligaments between neighbouring voids. Here some voids may collapse to micro-cracks, while other voids show a growing void volume.

The effect of the initial void size has been considered by analysing materials with a factor two between the initial void radii. Before void collapse in cases subject to low stress triaxiality or before the onset of necking under higher stress triaxiality, the materials with smaller voids can carry higher stresses, but later on there is not much difference in the response. Materials with big difference between the initial size of the two types of voids show initially a behaviour between that for both voids small and that for both voids large. Later, when the voids have either become micro-cracks or ligament necking has started, there is again not much difference.

Since the deformed unit cells found in the present analyses for low stress triaxiality do not indicate a failure mode, the possibility of bifurcation into a shear band has been considered. An approximate shear band analysis like that in Tvergaard (2014) has been attempted by searching for a periodic pattern of deformations with some shear, which could represent the deformations inside a shear band. However, no such bifurcation has been found by this method. This leads to the question whether or not it is plausible that there would not be a shear band instability in a material

subject to the overall stress state $\Sigma_{11}/\Sigma_{22} = -1.0$, with many cracks parallel to the principal tensile stress direction. All these cracks are closed with a high compressive stress similar to the transverse principal stress, and thus the material in this stress state does not really feel the presence of the cracks. The situation may be considered somewhat similar to a long fibre reinforced composite under tension in the fibre direction, with a very soft matrix material between the fibres. For such composites there would be no shear band instability under tension, whereas under compression fibre buckling or kink band instabilities could occur (Fleck, 1997).

One might think of failure due to nucleation of a second population of smaller voids in the material. But it seems likely that such voids would behave the same way as the voids analysed in the first place, which would indicate that a higher number of closed cracks parallel to the principal tensile stress direction would develop, all with a high normal compressive stress on the crack surfaces of magnitude similar to that of the transverse principal stress.

Even though the material with long closed cracks parallel to the principal tensile stress direction does not indicate a failure mode under low stress triaxiality, this material would be very sensitive to a change of stress state. If the transverse compressive stress is reduced to zero, failure can occur rapidly by necking of the long thin bars. If a macroscopic shear stress is applied, the material will have very little stiffness, as this will result in bending of the long thin bars.

It is finally noted that the prediction of shear bands would be very sensitive to an assumption that the metal forms a vertex on the yield surface. The same would be true for most other studies of void deformations, where large strains usually develop, so that relatively early shear localization would be predicted in the material near voids.

The initial void patterns analysed here have a high degree of symmetries, which are maintained during the large deformations, even when all voids develop into micro-cracks. It will be of interest in coming studies to consider the effect of other types of initial imperfections with fewer symmetries, subject to stress states in the vicinity of pure shear, like those considered in the present studies.

References

- Bao, Y., Wierzbicki, T., 2004. On fracture locus in the equivalent strain and stress triaxiality space. *Int. J. Mech. Sci.* 46, 81–98.
- Barsoum, I., Faleskog, J., 2007a. Rupture mechanisms in combined tension and shear – Micromechanics. *Int. J. Solids Struct.* 44, 5481–5498.
- Barsoum, I., Faleskog, J., 2007b. Rupture mechanisms in combined tension and shear – Experiments. *Int. J. Solids Struct.* 44, 1768–1786.
- Beese, A.M., Luo, M., Li, Y., Bai, Y., Wierzbicki, T., 2010. Partially coupled anisotropic fracture model for aluminum sheets. *Eng. Fract. Mech.* 77, 1128–1152.
- Benzerga, A.A., Leblond, J.-B., 2010. Ductile fracture by void growth to coalescence. *Adv. Appl. Mech.* 44, 169–305.
- Christoffersen, J., Hutchinson, J.W., 1979. A class of phenomenological corner theories of plasticity. *J. Mech. Phys. Solids* 27, 465–487.
- Dahl, J., Nielsen, K.L., Tvergaard, V., 2012. Effect of contact conditions on void coalescence at low stress triaxiality shearing. *J. Appl. Mech., ASME* 79 (2). Art. No. 021003.
- Dunand, M., Mohr, M., 2011. Optimized butterfly specimen for the fracture testing of sheet materials under combined normal and shear loading. *Eng. Fract. Mech.* 78, 2919–2934.
- Fleck, N.A., 1997. Compressive failure of fiber composites. *Adv. Appl. Mech.* 33, 43–117.
- Garrison Jr, W.M., Moody, N.R., 1987. Ductile fracture. *J. Phys. Chem. Solids* 48 (11), 1035–1074.
- Ghahremaninezhad, A., Ravi-Chandar, K., 2013. Ductile failure in polycrystalline aluminum alloy Al 6061-T6 under shear dominant loading. *Int. J. Fract.* 180, 23–39.
- Haltom, S.S., Kyriakides, S., Ravi-Chandar, K., 2013. Ductile failure under combined shear and tension. *Int. J. Solids Struct.* 50, 1507–1522.
- Hill, R., 1970. Constitutive inequalities for isotropic elastic solids under finite strain. *Proc. R. Soc. London A314*, 457–472.
- Hill, R., Hutchinson, J.W., 1975. Bifurcation phenomena in the plane tension test. *J. Mech. Phys. Solids* 23, 239–264.
- Hutchinson, J.W., 1973. Finite strain analysis of elastic–plastic solids and structures. In: Hartung, R.F. (Ed.), *Numerical Solution of Nonlinear Structural Problems*. ASME, New York, p. 17.
- Nahshon, K., Hutchinson, J., 2008. Modification of the Gurson model for shear failure. *Eur. J. Mech./A Solids* 27, 1–17.
- Nielsen, K.L., Dahl, J., Tvergaard, V., 2012. Collapse and coalescence of spherical voids subject to intense shearing: studied in full 3D. *Int. J. Fract.* 177, 97–108.
- Pedersen, T.O., 1998. Remeshing in analysis of large plastic deformations. *Comput. Struct.* 67, 279–288.
- Song, D., Agoras, M., Ponte Castañeda, P., 2015. The evolution of pore shape and orientation in plastically deforming metals: implications for macroscopic response and shear localization. *Mech. Mater.* (in press).
- Stören, S., Rice, J.R., 1975. Localized necking in thin sheets. *J. Mech. Phys. Solids* 23, 421–441.
- Tvergaard, V., 1976. Effect of thickness inhomogeneities in internally pressurized elastic–plastic spherical shells. *J. Mech. Phys. Solids* 24, 291.
- Tvergaard, V., 1990. Material failure by void growth to coalescence. *Adv. Appl. Mech.* 27, 83–151.
- Tvergaard, V., 1997. Studies of void growth in a thin ductile layer between ceramics. *Comput. Mech.* 20, 186–191.
- Tvergaard, V., 2008. Shear deformation of voids with contact modeled by internal pressure. *Int. J. Mech. Sci.* 50, 1459–1465.
- Tvergaard, V., 2009. Behaviour of voids in a shear field. *Int. J. Fract.* 158, 41–49.
- Tvergaard, V., 2012. Effect of stress-state and spacing on voids in a shear-field. *Int. J. Solids Struct.* 49, 3047–3054.
- Tvergaard, V., 2014. Bifurcation into a localized mode from non-uniform periodic deformations around a periodic pattern of voids. *J. Mech. Phys. Solids* 69, 112–122.
- Tvergaard, V., 2015. Effect of initial void shape on ductile failure in a shear field. *Mech. Mater.* (accepted for publication).
- Tvergaard, V., Hutchinson, J.W., 1981. Shear band formation in plane strain. *Int. J. Solids Struct.* 17, 451–470.
- Tvergaard, V., Nielsen, K.L., 2010. Relations between a micro-mechanical model and a damage model for ductile failure in shear. *J. Mech. Phys. Solids* 58, 1243–1252.